Multi-omic ADNI CSF and plasma data integration identifies distinct metabolic transitions in disease progression in Alzheimer's Disease

Tom Paterson[1], Jennifer Rohrs[1], Timothy J. Hohman[2], Mark Mapstone[3], Allan I. Levey[4], LeRoy Hood[5], Alzheimer's Disease Neuroimaging Initiative*, Cory C. Funk[1,5]

[1] Fulcrum Neuroscience, Palo Alto, CA
[2] Department of Neurology, Vanderbilt University
[3] Neurology at the UC Irvine School of Medicine
[4] Department of Neurology at Emory University's School of Medicine
[5] Institute for Systems Biology, Seattle, WA
*Data used in preparation of this article were obtained from the Alzheimer's Disease Neuroimaging Initiative (ADNI) database (adni.loni.usc.edu). As such, the investigators within the ADNI contributed to the design and implementation of ADNI and/or provided data but did not participate in analysis or writing of this report. A complete listing of ADNI investigators can be found at: http://adni.loni.usc.edu/wp-content/uploads/how_to_apply/ADNI_Acknowledgement_List.pdf

Email: cory.funk@isbscience.org, tpaterson@fulcrumneuro.com

Abstract

Age and APOE allele status are the two greatest risk factors for Alzheimer's disease, with microglial processing, recycling of debris and cholesterol transport emerging as other key genetic determinants from AD GWAS. How risk factors contribute to neuronal loss is an unanswered question. Using the ADNI dataset, we provide evidence for distinct processes driving neurodegeneration in AD across a range of ADAS13 scores binned into quartiles (Q1-4) found in ADNI. In Q1 individuals, we see evidence of white matter hyperintensities (WMH) associated with complement and HDL proteins, independent of tau and hippocampal atrophy rates. In Q2 individuals, we see specific protein/lipid correlation networks that are associated with tau and hippocampal atrophy. Also in Q2, we see variations in enzyme levels (LPA2G7, LPCAT2) that impact phosphatidylcholine availability for cholesterol efflux onto CNS lipoproteins. Low LPA2G7 and high LPCAT are associated with lower disruption of ANLS, while high LPA2G7 and low LPCAT are associated with higher disruption. In Q3 individuals, DHA and plasmalogens appear to be protective of astrogliosis, presumably by decreasing lipid droplet size, and increasing their lipid debris flux capacity. The networks we identify in this analysis provide evidence that progressively elevated cellular cholesterol levels, likely the result of accelerating neuronal and myelin debris, are perturbing homeostatic processes, resulting in disruption of astrocyte-neuron lactate shuttle (ANLS), contributing to lipid droplet formation, and astrogliosis. Existing studies have already identified elevated cellular cholesterol as the driver of increased access of APP to β- and γ-secretase for β-amyloid production in late-onset AD. Importantly, we provide evidence that points to actionable variations in lipids associated with slower disease progression and decreased metabolic disruption and inflammation. We believe this positive feedback loop (neurodegeneration → lipid debris processing → metabolic disruption → neurodegeneration) is a key destabilizing cycle responsible for disease progression in AD, reinforcing the perspective that Alzheimer's is fundamentally a metabolic disease. Our findings are consistent with established lipid risk factor associations. We anticipate the mechanistic insights from our analysis will advance nutritional and pharmacological interventions and slow cognitive decline.

Introduction

Alois Alzheimer first described the neuropathology that came to define the eponymous disease with his observations of neurofibrillary tangles, amyloid plaques, and lipid droplets[1]. Our modern

understanding of the disease is rapidly improving, driven in part by a recognition of the increasing cost of care. Presently, anti-amyloid therapies with ~35% effect size equate to extending one's dementia-free life by ~6 months[2]. Improved, personalized treatments are predicated on increased understanding of disease etiology. The two greatest risk factors for AD are age and APOE allele status[3]. GWAS studies have additionally identified loci associated with genes in processes involving processing of cellular debris such as phagocytosis, cholesterol metabolism, and innate immunity[4].

Alzheimer's first reported "many glial cells show adipose saccules," which are now known as lipid droplets, primarily by microglia, containing esterified cholesterol, triglycerides and phospholipids[5]. Lipid droplets alone are not indicative of pathology, and serve a temporary storage for lipids, including phagocytized cell debris, and are part of normal lipid homeostasis[6]. Cholesterol transport, synthesis, and homeostasis are tightly regulated in the brain where cholesterol can be synthesized and modified, with excess cholesterol being exported out of the CNS during sleep through reverse cholesterol transport (RCT) and/or conversion to 24-hydroxycholesterol (24OHC) or 27-hydroxycholesterol (27OHC), both of which can cross the blood brain barrier and are converted to bile acids in the liver. As cells themselves contain cholesterol, processing of dying cells and myelin turnover depends on cholesterol turnover and trafficking. When microglia become overwhelmed with this task, they signal for astrocytes to assist them through astrogliosis. In both microglia and astrocytes, a key mechanism that enables off-loading excess cholesterol via lipoproteins for RCT is activation of LXR which triggers lipid droplete lipophagy, and upregulates ABCA1 and APOE mRNA expression[7–10]. When lipid droplets become too large, they are unable to be transported to the mitochondria where CYP27A1 hydroxylates cholesterol into 27OHC, the key activator of LXR. In microglia, this results in the inability to off-load cholesterol onto lipoprotein particles[10,11]. In astrocytes, the same problem occurs, but the lack of 27OHC also fails to down-regulate LDLR-mediated cholesterol uptake and cholesterol biosynthesis via INSIG1 and SREBP2[9,12,13]. This lack of 27OHC leads to elevated cholesterol levels across all cellular membranes, including the plasma membrane where lipid raft function and GPCR signaling are affected[14–17].

GPCR signaling on astrocytes triggers lactate release in response to metabolic signaling from neurons. This signaling is part of a closed-loop system known as the astrocyte-neuron lactate shuttle (ANLS), which occurs at the nodes of Ranvier and synaptic boutons[18–20]. Because GPCR signaling and downstream ANLS are sensitive to astrocyte membrane cholesterol levels, multiple feedback loops (such as SREBP2 and LXR) exist to keep cholesterol levels at an optimal range[14,15,17,21,22].

Many of the molecular underpinnings around lipid homeostasis, LDs and inflammation in glial cells were described in recent work by Victor *et al* and Haney *et al*[23,24]. Using glial cell culture systems, they demonstrated how the overall levels of cellular cholesterol, either stored in lipid droplets, processed in the ER or golgi, or in extracellular lipoprotein particles, are increased by APOE4. Both groups demonstrate that inflammation from fAβ and/or other TLR4 activators causes a shift towards glycolysis, away from oxidative phosphorylation of fatty acids, and an increase in ACSL1 to store the fatty acids in lipid droplets. TCW *et al* showed that this increase in lipid droplets and impaired cholesterol efflux could be remedied by the addition of LXR agonists[25]. A conclusion from these papers was that the overall increase in the amount of glial cellular lipids contributes to neurotoxicity, presumably through an increase in the amount of extracellular lipid particles that are available to neurons in the media.

While these cell culture systems have been hugely insightful for elucidating the mechanisms of lipid storage, the role of fAβ, and the role of APOE in Alzheimer's etiology, a key limitation is that they do not recapitulate the recycling of cellular and myelin debris typically performed by microglia and astrocytes in vivo, nor do they properly model the diurnal pattern of reverse cholesterol transport in glial cells and neurons–essential to brain metabolism and homeostasis. For example, the importance of

signaling pathways involved in debris processing by TREM2 have been well studied, and are known to impact cholesterol biosynthesis[26].

We hypothesize that a key dynamic of AD pathophysiology is the flux capacity of microglia for processing cellular and myelin debris. Once this capacity is reached, and astrocytes are recruited to help with processing of excess debris, astrocytes' ability to provide metabolic support for neurons via ANLS is impaired, creating a negative feedback loop of neuronal death.

In support of this hypothesis, we find evidence in ADNI for distinct processes occurring in windows of disease progression corresponding to ADAS13 scores. The first signal we identify is a role for complement and HDL particles in cognitively normal individuals. We next observe a disruption in ANLS and a compensatory upregulation of glycolysis, in connection with elevated cellular cholesterol. Finally, we observe increased astrogliosis and a reduction in plasma acylcarnitines and cholesterol esters, implying reduced lipid flux out of the CNS. We interpret this change in lipid and protein correlation to indicate the point at which microglia reach their flux capacity for debris processing, thus recruiting and activating astrocytes, increasing astrocyte cholesterol levels, thereby further reducing neuronal metabolic support by ANLS.

RESULTS

Data Selection/Organization

While ADNI is a longitudinal dataset, baseline data for ADNI subjects varies, and does not include any longitudinal measurements for either the mass spec or Somascan CSF proteomics, with the baseline for any given individual being anywhere from cognitively normal to demented. As such, a given individual may or may not transition to demented over time. We thus opted for a cross sectional approach, using only baseline data. Additionally, as is well known in AD, in an attempt to remain cognitively normal, the brain engages in many compensatory strategies. Thus, by the time cognitive symptoms manifest, 30% of hippocampal volume is lost. At the cellular level, there are also known metabolic changes that occur and clearance of cellular debris from dying neurons. We hypothesized that these changes would be evident in the proteomic and lipidomic data, and that the capacity to handle such stresses would vary across individuals, all of which vary over time, and contribute to changes in disease pathology and stratification.

We grouped individuals based on their ADAS13 scores, a more continuous measure relative to disease progression identifiers. This enables us to better stratify “cognitively normal” individuals into two groups, and provide a finer lens of disease progression/etiology. We chose the CSF MS proteomics set of 48 proteins as our primary index for identifying lipid-protein correlations, as these proteins were selected as being the most differentially expressed between post-mortem AD and CN brain tissue samples, as well as on known CSF protein content.

We also selected individuals for whom both untargeted baseline plasma lipidomic data[27], and targeted baseline CSF proteomic data[28] existed. The CSF proteomics are a set of 48 proteins chosen based on their observed differential expression between case and control among postmortem brain samples[28]. We also identified individuals, for whom CSF Somascan proteomics[29], and/or Nightingale plasma lipoproteins were available. A venn diagram of the sample overlap for all the data modalities used is found in **figure 1.**

We grouped individuals into quartiles based on their ADAS13 scores (**figure 1B)**. Out of a total of 2,428 ADNI subjects (ADNI, ADNI2, ADNI GO), 1,384 patients contained longitudinal lipidomics data, 602 of whom also had baseline CSF proteomics. Individuals for whom there were plasma lipidomics, CSF proteomics and CSF Somascans totaled 362, and individuals for whom there were plasma lipidomics, CSF proteomics and Nightingale lipoproteins totaled 601.

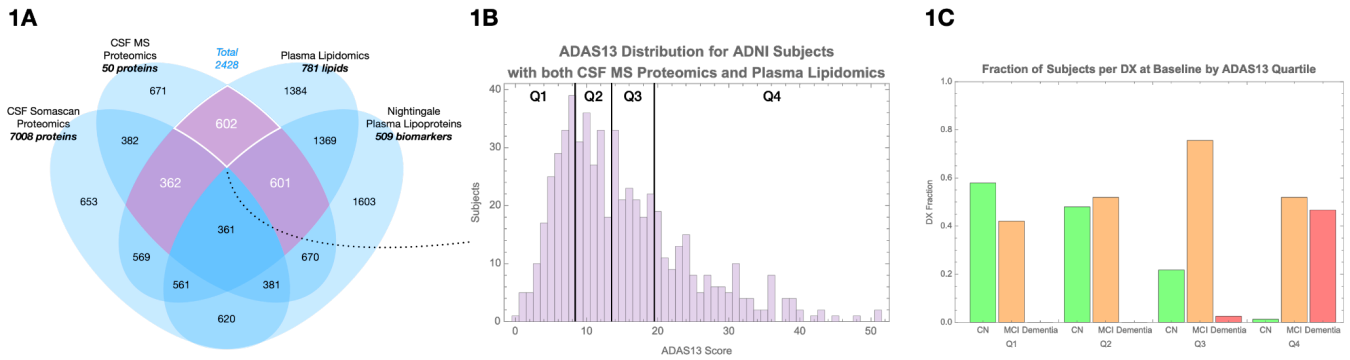

Figure 1: A) *Schematic representation of ADNI data used for analysis.* **B)** ADNI individuals with both CSF MS proteomics and plasma lipidomics, spanning cognitively normal to demented were selected for subsequent analyses. **C)** Distribution of clinical diagnoses across ADAS13 quartiles.

Reasoning that the 48 mass spec CSF proteomics might better represent disease progression changes in the brain, we explored correlations between 781 plasma lipids 48 mass spec CSF proteins between cognitively normal and MCI/AD, separating the samples into quartiles (Q1 = 1-7; Q2 = 8-12; Q3 = 13-18; Q4 = 19-52), respectively, spanning a range of cognitively normal, through MCI and demented. As ADAS13 scores do not have a perfect overlap with clinical diagnosis in ADNI, we show in **figure 1C** the distribution of diagnoses within each quartile. Even with the imperfect overlap, the diagnoses align with what we would expect for the ADAS13 quartiles. We then performed inter-omic correlations for both the CSF proteins and lipids. Strikingly, we observe significant differences between each quartile, with visible changes and patterns in each, with blue representing negative correlations, and orange representing positive correlations (**figure 2**). The most visually striking change we observed was found in Q3. These results identify clear changes in correlations between the CSF proteins and plasma lipids for each of the quartiles, providing a rich, multiomic canvas to explore stage-specific changes of disease progression.

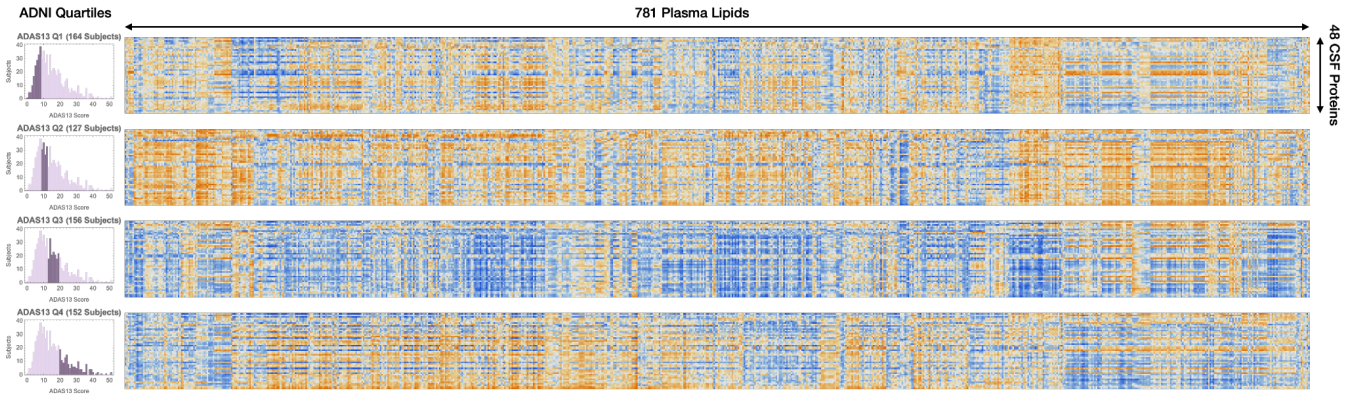

Figure 2: Selected ADNI individuals were divided into quartiles based on their ADAS13 distribution. Interomic protein and lipid correlations are represented by quartile in a heat map with blue correlations being negative and orange correlations being positive.

To better understand the observed inter-omic changes in each quartile, we performed a separate cluster analysis for the proteins and lipids. This resulted in three groups of proteins and ten clusters of lipids, the contents for each can be found in **supplemental table 1**. We used naming convention based on the lipid cluster's most prevalent head group and fatty acid (or the first and second

if the second's prevalence is more than 2/3rds the first). For the proteins, three clusters emerged. The second protein cluster contained several lipoproteins and complement cascade proteins. We named this group “complement/HDL.” The third cluster contained proteins associated with hemoglobin, which we named “hemoglobin.” The first cluster contained significantly more proteins than the other two, so we functionally subdivided this protein cluster into groups based on their established functions. This resulted in 5 subgroups: astrogliosis, astrocyte-neuron lactate shuttle (ANLS) / glycolysis, hypoxia, synapses, and phagocytosis.

To improve statistical power, we combined the protein clusters and lipid clusters using principal component analysis and performed interomic correlations. We calculated the correlations for the first principle components (FPC) of each protein/lipid pair. Consistent with the striking visual change we saw in the individual protein/lipid correlations in Q3 (**figure 2**), we observed a wide band of significant cluster FPC correlations across multiple protein clusters with a single lipid cluster, phospholipids| plasmalogens 22.6 (**figure 3**). This lipid cluster contains a mix of phospholipids and cholesterol esters. Twenty three of the 28 phospholipids are plasmalogens, and all phospholipids have either docosahexaenoic acid (DHA) or eicosapentaenoic acid (EPA). Similarly, each cholesterol ester contains either DHA or EPA (**supplemental table 1A**). DHA and EPA are also known as omega-3s, making 34 of the 35 lipids in this group omega-3s.

Surprisingly, this analysis also revealed a significant FPC cluster correlation in Q1, with the hexceramides | phospholipids, seemingly independent of the visual change in figure 2, Q3. Leveraging additional ADNI biomarkers other than those used for the clustering, we investigated specific protein cluster/lipid cluster correlations for each quartile.

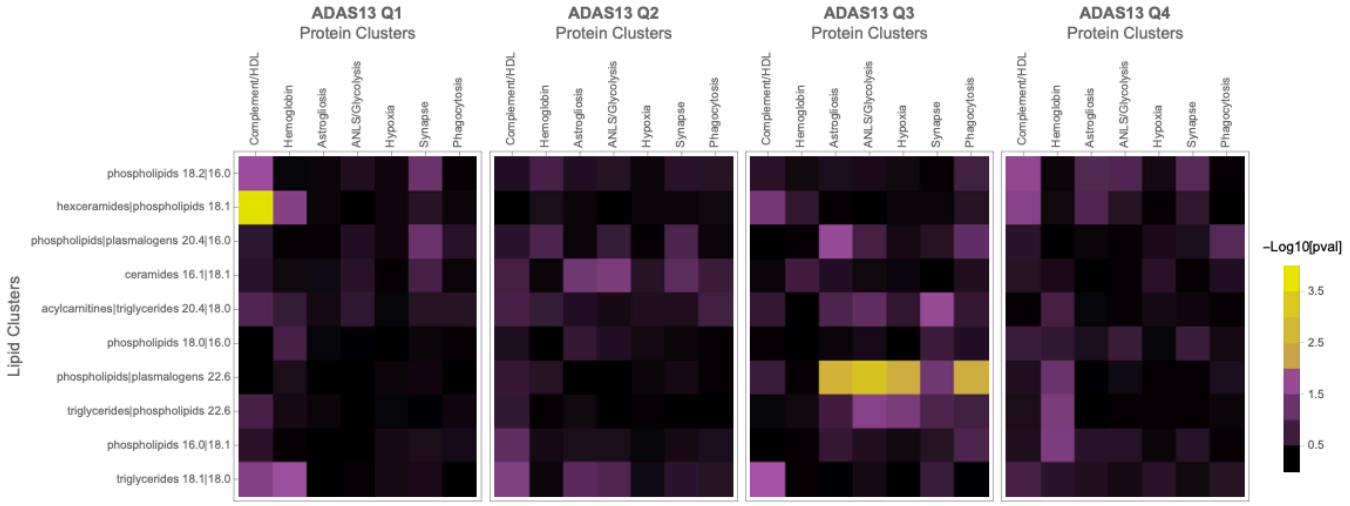

Figure 3: First principle components for protein (x-axis) and lipid (y-axis) clusters were correlated for each quartile and represented as a heatmap with the most significant correlations being yellow.

Quartile 1 Analysis

We observed significant (pvalue 1.2E-5) correlations between the hexceramide|phospholipid 18.1 cluster with the complement/HDL protein cluster, containing the following proteins: ALB, APOA4, APOC1, APOC2, CP, C9, KNG1, PGLYRP2, PON1, THRB (**figure 3, Q1 panel**). We looked for differences among the first quartile individuals with respect to biomarkers, splitting the individuals based on quadrants from the scatter plot (**figure 4A**). We observed differences in white mater hyperintensities (WMH), with the greatest difference between the top left quadrant (high hexceramides; low complement/HDL) and bottom right quadrant (low hexceramides; high complement/HDL) (**figure 4B**).

These differences could be attributable to both axes, as comparisons between the left and right (low vs high complement/HDL proteins) were similar, as were top vs bottom (low vs high hexceramides). The greatest difference in WMH (top left vs bottom right) was 2.00/3.42, or a 58% increase. Individuals with high hexceramides and low levels of complement/HDL proteins had much lower WMH values. Interestingly, the top left quadrant was predominantly female (56/63 individuals; 0.89%)(**supplemental figure 1A**). A previous report identified sex differences in ceramide (but not hexceramide) levels and WMH[30,31]. We thus looked to see if we observed any sex differences in WMH (**supplemental figure 1B**), and did not see any statistically significant differences, though we cannot rule out a sex-specific difference.

With the observed changes in WMH, we next looked at the SomaScan proteomics data using a similar approach of comparing quadrants. With 164 individuals, we compared protein expression between the left and right quadrants (high vs low of the original CSF complement/HDL protein cluster). Using cutoffs of 0.25 Log2 fold change and p-value< 0.001, we identified 72 Proteins (**figure 4C**, **supplemental table 2A)**. Using EnrichR, we similarly identified the *Complement and coagulation cascade* pathway, with the most significant adjusted p-value being 6.2e-27, consistent with our original CSF proteomic functional identification (**s table 2B**). To better understand the axis of variation for the hexceramides, we compared the SomaScan proteomics for the top vs bottom. With cutoffs of 0.15 Log2 fold change and p-value < 0.001, we identified 49 proteins (**figure 4D**, **supplemental table 3A**). The pathway with the greatest significance was *Alternative Complement Pathway* with an adjusted p-value of 3.3e-4 (**supplemental table 3B**).

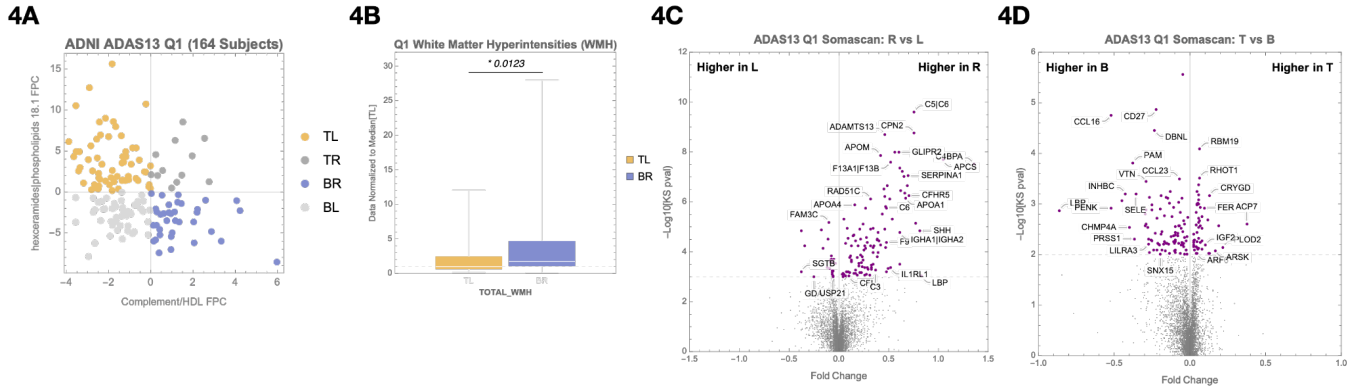

Figure 4: Quadrant analysis of ADAS13 Q1**. 4A)** Scatter plot of *individuals represented across Complement/HDL protein cluster (x-axis) vs hexceramide|phospholipid 18.1 lipid cluster (y-axis).* ***4B)*** *Box-whisker plots of white matter hyperintensities in TL vs. BR quadrants.* ***4C)*** *SomaScan volcano plots for R vs. L quadrants.* ***4D)*** *Top vs. bottom quadrants.*

Quartile 3 Analysis

Astrogliosis protein cluster

We observed a strong protein/lipid signal in Q3 between the astrogliosis protein cluster, containing proteins YWHAB, YWHAZ, CHI3L1 and CD44, and the lipid group containing phospholipids | plasmalogens 22.6. CHI3L1 and CD44 interact as receptor-ligand[32], are associated with neuroinflammation and disease progression and correlate well with the astrogliosis marker GFAP[33]. YWHAB and YWHAZ both bind to GFAP and are also associated with activated astrocytes[34,35]. To better understand the differences and processes responsible for individuals within Q3, we plotted individuals based on their FPC for astrogliosis proteins on the x-axis, and phospholipids | plasmalogens 22.6 on the y-axis (**figure 5A**). From the resulting quadrants, individuals in the bottom-right had a median increase of 55% Tau levels compared to individuals in the top-left (**figure 5B**). Consistent with

these findings, individuals with higher astrogliosis protein expression (bottom-right) had a median increase hippocampal atrophy rate of 92% (**figure 5B**). We also observed an increase in the established astrogliosis marker GFAP in the Somascan data (**figure 5B**).

As part of normal lipid homeostasis, fatty acids, cholesterol and other lipid species become esterified and stored in lipid droplets, with PI3K activation substantially increasing this process, and increasing the size of the lipid droplets. Large lipid droplets are less able to be transported to mitochondria by the actin cytoskeleton, where their cholesterol load is partially metabolized by CYP27A1 (found exclusively on the inner membrane of mitochondria) into 27OHC, and acyl-CoA from LD neutral lipid breakdown is metabolized to acylcarnitines. We looked for evidence of this in Q3 by comparing the lipids in the top-left quadrant of Q3 with those in the bottom-right. Of the 35 acylcarnitines in the lipidomic data, we found 7 acylcarnitines to be significantly different between the two quadrants with all of them trending in the expected direction, including both the DHA and EPA species (**figure 5B**). We see a similar pattern in cholesterol esters. Of the 39 cholesterol esters, we found 11 to be significantly different between the two quadrants, all of them trending in the expected direction (**figure 5B**). This quadrant-specific cholesterol ester data is echoed in Nightingale HDL markers for cholesterol and cholesterol esters in XL.HDL particles (**figure 5C**), a size class consistent with the sized observed in CNS lipoproteins from post-mortem AD patients[36]. Interestingly, HDL3 cholesterol levels are also elevated in the top-left quadrant **(figure 5C**).

Together, our observations of the bottom-right vs. top-left individuals are consistent with reduced LD processing (acylcarnitines) and cholesterol efflux (cholesterol esters) out of the brain, into the plasma, at the same time when neuronal loss is known to occur in the hippocampus (hippocampal atrophy) and temporal cortex[37]. Considering mass balance, with fewer lipids exiting the brain, coupled with known neuronal loss, and the known role of microglial phagocytosis, these data point to an accumulation of neuronal debris in microglia and/or astrocytes, reflective of the known accumulation of LDs in Alzheimer's. Furthermore, individuals in the bottom right, where more neuronal death is occuring (greater tau), display even less cholesterol efflux, whereas individuals in the top left, while still progressing with the disease, display greater efflux.

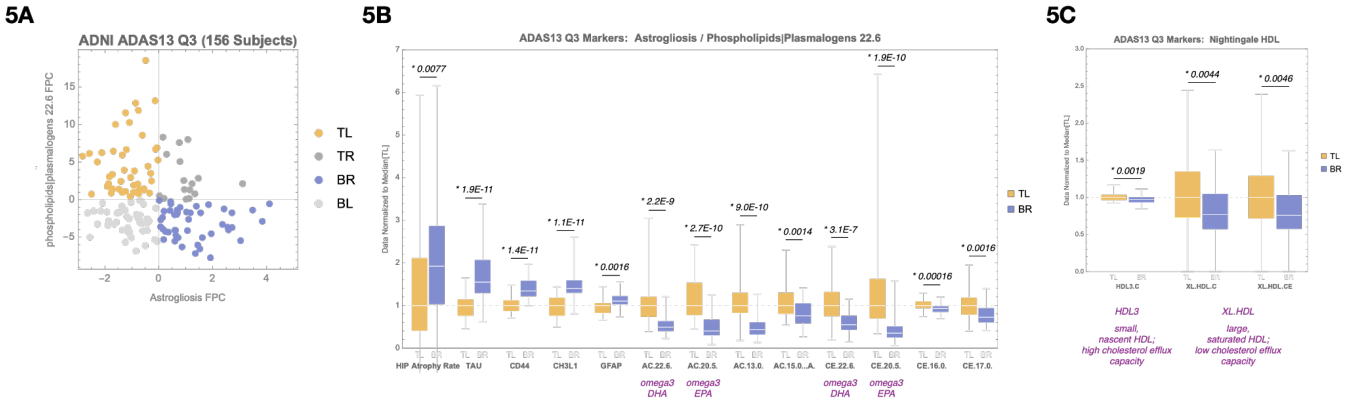

Figure 5: *Quadrant analysis of ADAS13 Q3.* ***5A)*** *Astrogliosis protein cluster (x-axis) vs phospholipids | plasmalogens 22.6 lipid cluster (y-axis).* ***5B)*** *Box whisker plots comparing TL vs. BR for markers of disease progression (hippocampal atrophy rate, tau), astrogliosis (CD44, CH3L1, GFAP), beta oxidation (omega 3 and non-omega 3 acylcarnitines) and reverse cholesterol transport (omega 3 and non-omega 3 cholesterol esters).* ***5C****) Box whisker plots comparing TL vs. BR for significant Nightingale HDL lipoprotein markers (HDL3, XL.HDL.C, XL.HDL.CE).*

ANLS/glycolysis protein cluster

The strongest protein/lipid signal in Q3 occurred between the ANLS/glycolysis proteins (LDHB, LDHC, CD44, ALDOA, PKM, MDH1, GAA, ENO1) and the lipid group containing phospholipids | plasmalogens 22.6. The most significant FPC protein correlation coefficient was with ANLS/glycolysis at a p-value of 2.0e-3. Among the lipids and proteins that make up the FPCs, several individual correlations had significant p-values, as shown in **figure 6B**. To better understand the differences and processes responsible for individuals within Q3, we plotted individuals based on their FPC for ANLS/ glycolysis proteins on the x-axis, and phospholipids | plasmalogens 22.6 on the y-axis (**figure 6A**). From the resulting quadrants, individuals in the bottom-right had a median increase of 65% Tau levels compared to individuals in the top-left (**supplemental figure 3**). This is consistent with the idea that high levels of omega-3s are protective of metabolic stress, as indicated by high levels of ANLS/ glycolysis proteins (and higher Tau).

As omega-3 are most commonly associated with brain health[38,39], and reduce microglial polarization[40], researchers have created an omega-3 index to help provide a standard quantitative assessment of omega-3s in the body[41]. We utilized the Nightingale data to approximate the omega-3 index[42]. Nightingale consists of an array of lipoprotein particle size measurements and lipid compositions. The recommended omega-3 index range is between 8-11[43]. The median for individuals in the top-left quadrant were within range (>8.0), while the median for individuals in the bottom-right quadrant was lowest at 6.7 (**figure 6C**). This was a significant difference with a p-value of 8.6e-7.

Individuals in the lower-left quadrant had similarly low levels of Tau relative to individuals in the top-left, in spite of low omega-3 levels (**supplemental figure 3**). To identify potential explanations for this, we compared the lipidomic levels of all individuals between the left and right quadrants (low vs high levels of the ANLS/glycolysis proteins)(**figure 6D**). We observed higher plasmalogens and a number of plasmalogen-precursors: monoalkyl-diacylglycerols, in individuals with lower expression levels of the ANLS/glycolysis proteins (**figure 6B**). Higher plasmalogens and higher omega-3 are both known to result in lipid droplets of a smaller size[44,45].

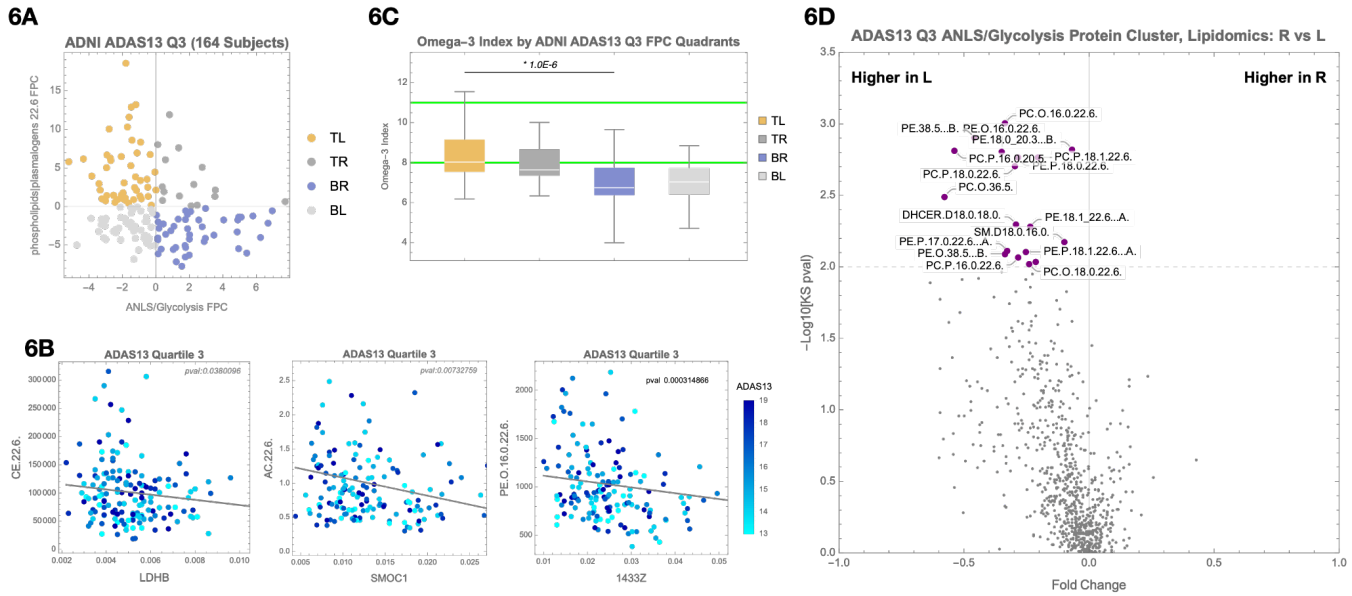

Figure 6: *Quadrant analysis of ADAS13 Q3.* ***6A)*** *ANLS/glycolysis protein cluster (x-axis) vs phospholipids | plasmalogens 22.6. lipid cluster (y-axis).* ***6B)*** *Scatter plots for the same Q3 subjects of several significant protein-lipid pairs (LDHB-CE.22.6., SMOC1-AC.22.6., 1433Z-PE.O.16.0.22.6.).* ***6C)*** *Box-whisker plots of estimated omega-3 index (based on Nightingale lipoprotein markers) by quadrants.* ***6D)*** *SomaScan volcano plots for R vs. L quadrants.*

Quartile 2 Analysis

Due to the observed changes in lactate shuttle/glycolysis in the Q3, we wondered if there were indications of change occurring in Q2. While no single protein-lipid cluster reached significance, the ANLS/glycolysis proteins and ceramides 16.1|18.0 had the best p-value. As we previously did for Q1 and Q3, we plotted individuals based on their FPCs for the protein and lipid clusters (**figure 7A**), and looked at the biomarker differences between the top-left and bottom-right. Once again, we found similar differences in hippocampal atrophy rate (trending) and Tau levels (significant), with a 59% difference in Tau between the two groups (**figure 7B**). Given the insignificant p-value for the cluster FPC correlation, we looked at individual lipid-protein pairs in this cluster and found two ceramides (CER.D19.1.18.0 and CER.D19.1.16.0) correlating at an order of magnitude better than any other lipid with all the proteins, including LDHB (p-values 0.0046 and 0.0069 respectively, compared to 0.02 to 0.04 for the next highest six ceramides) (**figure 7C**). We then looked in the SomaScan CSF proteomics for any proteins that correlated with CER.D19.1.18.0. and found 24 proteins with a p-value < 0.003 (**supplemental table 4**). EnrichR analysis of these proteins identified the *Bile acid and bile salt biosynthesis via 24-hydroxycholesterol* pathway, with an adjusted p-value of 6.1e-3. These same proteins showed little correlation with CER.D19.1.18.0. in Q1, and modest, but significantly less correlation with CER.D19.1.18.0. in Q3, supportive of a quartile-specific difference in cholesterol metabolism (**figure 7F**). Consistent with our identification of bile acid synthesis, propionyl-CoA, a rate limiting substrate for odd-chain fatty acid synthesis, is a product of bile acid synthesis from cholesterol and is used to make odd-chain fatty acids, including CER.D19.1.18.0..

With our inferred observation of increased bile acid synthesis connected with metabolic stress, and recent work by TCW et al[25] showing the importance of lipid transport mechanisms to the mitochondria for access to CYP27A1 and the alternative bile acid synthesis pathway, we reasoned that these steps for translocation may be subject to influence by genetic variants. We turned to established AD GWAS loci to look for any SNPs that are enriched for increased/decreased CER.D19.1.18.0 levels. Surprisingly, we found multiple loci associated with PICALM, TNIP1, INPP5D and TSPOAP (**supplemental figure 4**). Interestingly, each of these genes has an established function in cholesterol trafficking that can be related to CER.D19.1.18.0. PICALM is involved in vesicular trafficking of cholesterol to the mitochondria where CYP27A1 initiates the conversion of cholesterol to bile acids and propionyl-CoA[46]. TNIP1 inhibits NF-KB signaling which downregulates CYP27A1[41,42]. INPP5D negatively regulates PI3K/Akt signaling, increasing ABCA1 expression[47,48], and TSPOAP helps transport cholesterol from the outer to the inner mitochondrial membrane where CYP27A1 resides[49].

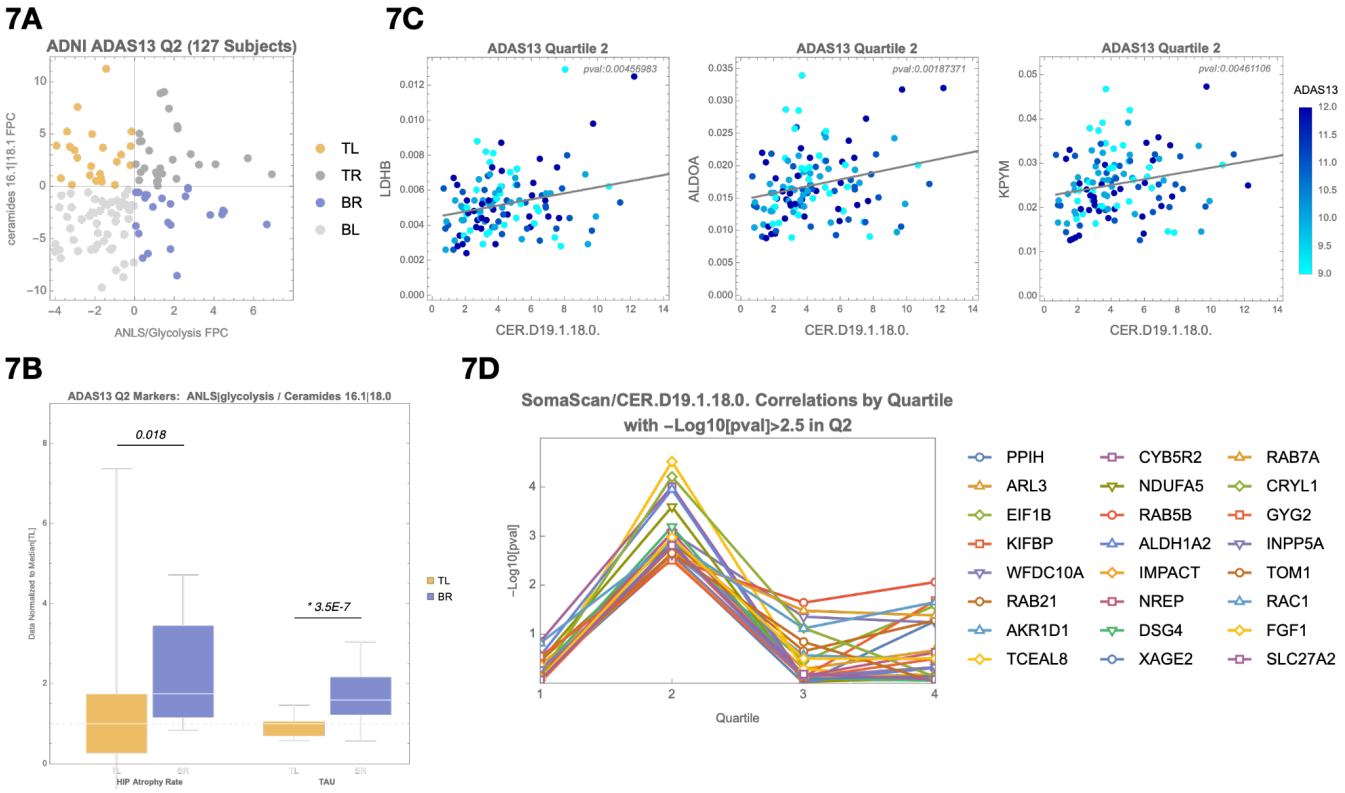

Figure 7: *Quadrant analysis of ADAS13 Q2.* ***7A)*** *ANLS|glycolysis protein cluster (x-axis) vs Ceramides 16.1|18.0 lipid cluster (y-axis).* ***7B)*** *Box-whisker plots of Q2 disease progression markers in TL vs. BR quadrants.* ***7C)*** *Scatter plots for Q2 subjects of several ANLS|glycolysis proteins (LDHB, ALDOA, KPYM) vs. CER.D19.1.18.0.* ***7D)*** *Q2-significant SomaScan CSF proteomics correlations with CER.D19.1.18.0. shown across quartiles.*

Having identified evidence for increased bile acid synthesis being correlated with metabolic stress in Q2, we looked for similar evidence of the other key mechanism for excess cholesterol clearance, efflux to CSF lipoproteins. We evaluated the lipid species between the top and bottom Q2 quadrants to characterize the lipid signature and noticed a number of lysophosphatidylcholine (LPC) lipid species as significant (**supplemental figure 5**). Phosphatidylcholine (PC) is a rate limiting reactant for free cholesterol esterification onto lipoproteins via ABCA1|LCAT, generating LPC in the process[50,51]. We then evaluated how the key enzymes involved in the interconversion of PC to LPC correlated with LDHB (**figure 8B**). We observed a significant positive correlation between plasma PLA2G7 and CSF LDHB (p-value = 4.04e-5) and a significant negative correlation between plasma LPCAT2 and CSF LDHB (p-value = 3.6e-3) (**figure 8A**). With elevated LDHB levels being an indicator of metabolic stress in neurons, high levels of LPCAT2 and low levels of LPA2G7 both correlate with lower levels of LDHB, presumably because of increased PC levels. As such, we see a correlation between PC-mediated cholesterol efflux and metabolic stress.

Among the other proteins that correlated with CER.D19, we found TNR and CNTN2, two cell adhesion proteins that can bind directly to each other and are known to facilitate communication between astrocytes and neurons at the Nodes of Ranvier and synapses–two sites at which astrocyte-neuron lactate shuttle (ANLS) occur[20,52]. We broadened our search to look for additional processes that are actively maintained as part of ANLS. This turned our attention to the levels of norepinephrine in the data. Epinephrine is the metabolic signal from neurons to astrocytes that regulates ANLS activity[20,53]. Norepinephrine is not found among the SomaScan proteins, but chromogranin (CHGA) is, which is co-

secreted with norepinephrine[54]. We found chromogranin to be highly correlated with all the glycolytic CSF proteins, including LDHB (**figure 8C,D**). All of these quartile 2 multi-omic correlations are summarized in the graph shown in **figure 8D**.

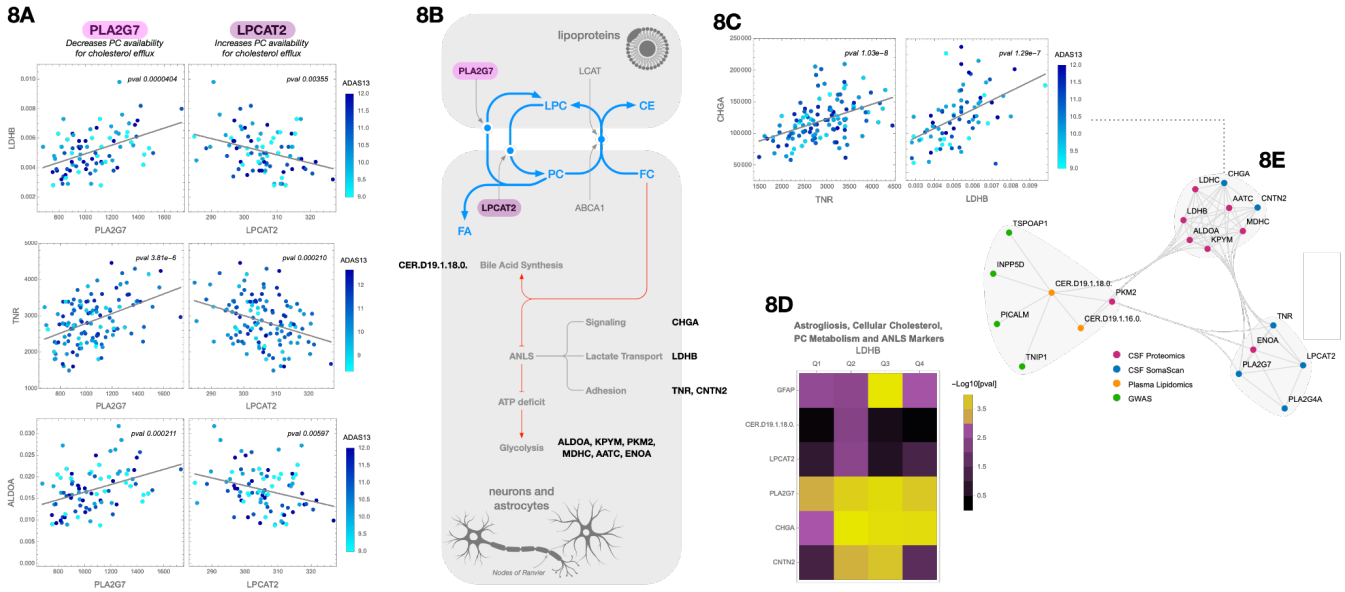

Figure 8: *Quartile 2 analyses relating cholesterol efflux, cellular cholesterol, ANLS, and metabolic stress.* ***8A)*** *Scatter plots of PC metabolism enzymes PLA2G7 and LPCAT2 vs. ANLS and glycolysis markers (LDHB, TNR, ALDOA) showing reciprocal correlations in agreement with the enzymes' activities on PC.* ***8B)*** *Schematic illustrating connectivity between PC metabolism, cholesterol efflux, bile acid synthesis, ANLS, and glycolysis.* ***8C)*** *Scatter plots showing strong correlations between CHGA with ANLS markers (LDHB, TNR) .* ***8D)*** *Heatmap showing changes in LDHB correlations with astrogliosis (GFAP), cellular cholesterol (CER.D19.1.18.0.) PC metabolism enzymes (PLA2G7 and LPCAT2) and ANLS signaling/adhesion markers (CHGA, CNTN2) as a function of ADAS13 quartile, showing evidence of elevated cholesterol and ANLS disruption beginning in Q2 prior to astrogliosis in Q3.* ***8E)*** *Summary graph of all observed correlations across CSF proteomics, plasma lipids, and genetics.*

Seeing correlations between LDHB (indicator of neuronal metabolic stress), homeostasis and astrogliosis, we wanted to observe these markers across all quartiles (**figure 8E**). We found GFAP to have the strongest correlation with LDHB in Q3, while we observed chromogranin (CgA) to correlate with LDHB earlier in Q2, continuing on through Q4. CNTN2, a marker of astrocyte-neuron communication, correlated with LDHB in Q2 and Q3, but not Q4. As with GFAP, the lack of correlation between CNTN2 and LDHB in Q4 might be due to excessive dysregulation of many signaling pathways. LPCAT2's correlation with LDHB was strongest in Q2, be it modest, while PLA2G7 correlated with LDHB in all quartiles.

Collectively, in Q2, we find evidence for proteins involved in ANLS/glycolysis that correlate with both cholesterol efflux and bile acid synthesis. We find contextual genetic evidence for AD GWAS variants correlating with CER.D19, which we find to be correlated with increased expression of the ANLS/glocolysis proteins. The correlations we identify are consistent with elevated cellular cholesterol, likely due to the processing/trafficking of neuronal debris. These data are resonant with the dysfunctions we observed in Q3.

Methods

ADNI Data

Data used in the preparation of this article were obtained from the Alzheimer's Disease Neuroimaging Initiative (ADNI) database (adni.loni.usc.edu). The ADNI was launched in 2003 as a public-private partnership, led by Principal Investigator Michael W. Weiner, MD. The primary goal of ADNI has been to test whether serial magnetic resonance imaging (MRI), positron emission tomography (PET), other biological markers, and clinical and neuropsychological assessment can be combined to measure the progression of mild cognitive impairment (MCI) and early Alzheimer's disease (AD).

ADNI Genetics

Genetic data from ADNI were cleaned and processed using Plink (version 1.9). Imputation was completed using the TOPMed imputation server, retaining high quality imputed variants (R^2>0.8). Quality control included removing variants for genotyping efficiency (<5%), low minor allele frequency (<1%), or out of Hardy-Weinberg equilibrium ($p<1x10^{-6}$). Samples were removed if their reported sex did not match their genetic sex, or if relatedness with another sample was identified (pi-hat>0.15). Finally, for the present analyses we used data from individuals of European ancestry based on a principal component analysis with the CEU population from 1000 Genomes used as a reference. A total of 1,414 participants and 7,953,272 variants passed all quality control procedures and were used in the present analyses[55].

Clustering and Principal Component Analysis

Clustering, principal component analysis, linear regressions, and statistical analyses were performed using Wolfram Mathematica v14.0.

Hippocampal Atrophy Rate Calculation

For each individual, hippocampal atrophy rate was calculated by linear regression over all available time points measures of hippocampus volume, and presented as percent per year normalized to volume at baseline.

Omega-3 Index Calculation

We calculated the omega-3 index based on the description found in Schuchardt and et al Schacky et al[56–59]. Briefly, we log-transformed the O3I and/or DHA% and non-DHA% prior to fitting a regression equation. The additive model containing two terms was determined to be the final prediction model, including β-coefficients for term: eO3I = 2·629 × NMR DHA% þ 0·4673 × NMR non-DHA% − 0·1014. The correlation of the eO3I vs observed O3I values was calculated for all ADNI individuals.

Discussion

By organizing the ADNI individuals by ADAS13 scores and performing inter-omic correlation between the plasma lipidomics and CSF proteomics we were able to identify what appear to be distinct transitions within each quartile. We further stratified individuals within each quartile to elucidate the combinations of lipids and proteins most responsible for the observed correlations. This approach helped us to better understand the drivers of change occurring within each quartile.

In the first quartile, we observed changes in the correlations between the complement/HDL proteins and hexceramides. These changes coincided with significant differences in WMH. Differences in WMH, as well as complement and several HDL proteins, have connections to breaches in the blood brain barrier (BBB)[60,61]. Lipoproteins such as APOC1, APOA4 have been found to associate with CP and C9[62]. C9 is a crucial subunit of the membrane attack complex, playing a vital role in innate and adaptive immune responses by creating pores in the plasma membrane of target cells[63,64]. Increased albumin (ALB) is often used as an indicator of compromised BBB[65]. Both albumin and APOA4 can bind

sphingosine 1-phosphate (S1P), which is a versatile lipid mediator essential for vascular development and lymphocyte trafficking[66]. KNG1 is a precursor for bradykinin, a peptide involved in inflammation and vasodilation. Bradykinin can increase BBB permeability by disrupting tight junctions between endothelial cells, contributing to inflammation-related BBB disruption[67,68]. PON1, an enzyme with antioxidant properties that can protect lipids from oxidation, also associates with HDL particles, whose by-products can react with reduced iron, generating 4-hydroxy-2-hexenal (4-HNE), which can damage neuronal membranes, alter tight-junctions and impair the BBB[69]. With these many connections to complement and other signaling pathways associated with lymphocytes, and the recent work by Chen *et al* that identified CD8+T cells as drivers of neurodegeneration in a tau mouse model, it is tempting to speculate that the initial events observed in Q1 might enable access of T cells to the brain[23]. An outstanding question remains as to what the drivers of these events might be, and if they are discernable from normal aging.

In Q2 and Q3, we observed patterns in lipids and proteins that we interpret to be due to variations in excess cellular cholesterol in neurons and glia. Recent work by Haney *et al* showed that both APOE and β-amyloid could increase cholesterol levels in the form of lipid droplets through activation of PI3K by TLR4 in a microglial cell culture system[70,71]. Independently, several other groups have shown the importance of the TREM2 pathway and the role of phagocytosis of cell and myelin debris[72]. While alterations in intracellular cholesterol location and amount are likely to be impacted by both PI3K and TREM2 signaling, our analysis points to increased phagocytosis of cell debris to be the primary source of excess cholesterol in microglial cells that cause them to reach their flux capacity limit, triggering astrogliosis, recruiting astrocytes to engage in phagocytosis[73]. Specifically, phagocytized debris are rich in membrane phospholipids, and we observed that individuals with higher levels of omega-3s fare better, having lower levels of tau and not reaching flux capacity. While we cannot rule out the possibility of de novo phospholipid synthesis in phagocytes (microglia, astrocytes), for the purpose of encapsulating cellular lipid debris in LDs, we believe this to be unlikely and even more metabolically expensive.

The evidence we present supports our hypothesis of coupling between debris processing, excess cellular cholesterol, and ANLS metabolic support (**figure 9**). We believe the underpinnings of this coupling relate to differences in the architecture of lipid trafficking in the CNS relative to the periphery. The periphery uses a two-particle class system: ApoB lipoproteins for distribution of resources (TG), and APOA1 lipoproteins for recycling of resources (cholesterol). An advantage of this two-particle system in the periphery is that the distribution and recycling operate independently and continuously. Contrast this with the CNS, which has a one-particle class system, where APOE is the primary apolipoprotein used for both resource distribution (transporting cholesterol from astrocytes to neurons) and recycling (redistributing excess cellular cholesterol and TG within the CNS, and removing lipid debris from the CNS via glymphatic clearance) (**figure 9A**). The consequences of this one-particle lipoprotein system are apparent in Haney et al, where they observe neuronal toxicity as a result of PI3K activation, down-regulating fatty acid metabolism, and increasing the amount of TGs that must then be off-loaded by APOE lipoproteins. The high levels of TG in these lipoprotein particles are then delivered to neurons where they are toxic.

A similar problem with this one-particle lipoprotein system occurs with regard to cholesterol transport. To avoid reabsorbing the very lipids intended to be removed from the CNS via the glymphatic system, this single-particle system functions as a timeshare, with numerous genes involved in LD sequestration and ABCA1-mediated cholesterol efflux being tightly tied to diurnal cycles/clock genes (**figure 9A**). This allows loaded HDL particles to be excreted/lipidated during sleep and avoids them from being recycled between cell types. We interpret our data to suggest that the capacity of this timeshare is overrun when excessive cellular debris must be processed on top of normal homeostatic cholesterol transport.

With astrocytes, neurons, and microglia all producing and consuming over-loaded lipoprotein particles in the CNS for both resource distribution and waste removal/recycling, this will naturally result in an elevated dynamic equilibrium of cholesterol levels in all cell types[74], systemically impacting membrane fluidity, cell signaling and metabolism[75](**figure 9B,C**). Elevated neuron cholesterol levels have been shown to drive β-amyloid production [76–78](**figure 9D**), so we see these processes operating upstream of amyloid pathology in late onset AD.

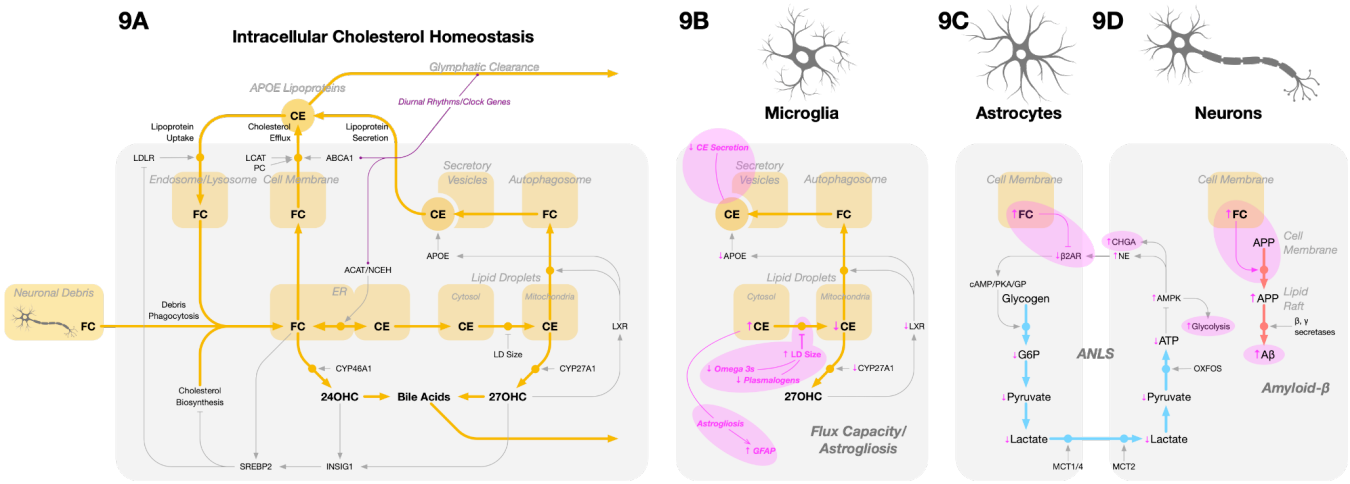

Figure 9: A) *Schematic depiction of intracellular cholesterol homeostasis and regulation in a one-particle class lipoprotein system for microglia, astrocytes and neurons. Consequences of cellular cholesterol overload due to excess cellular debris causing* ***B)*** *microglial flux capacity;* ***C)*** *disruption of ANLS in astrocytes;* ***D)*** *upregulated glycolysis in compensation to disrupted ANLS and increased access of APP to β- and γ-secretase in neurons.*

A key challenge in looking at the ADNI lipidomic and Nightingale data is that it's measured from the periphery, containing a mix of lipids from CNS glymphatic drainage and the periphery. This makes attributing the origin of any lipoprotein particles measured in the periphery difficult. What is known, from studies of HDL particles in the CSF, is that the XL_HDL particles in control individuals are much smaller than individuals with AD, with APOE4 alleles correlating with larger size[36]. HDL particle size helps determine the carrying capacity for cholesterol efflux out of the CNS[79]. Efflux capacity is negatively associated with particle size[80–82]. We find evidence in the lipidomic/proteomic correlations in Q2 and Nightingale lipoprotein particle size in Q3 that efficient cholesterol efflux is important for minimizing metabolic stress. In Q2, we find that PC availability to support cholesterol efflux improves metabolic stress as indicated by the correlations of LDHB/glycolytic proteins with the opposing activity of two enzymes (PLA2G7, LPCAT2) (**figure 8A**). In Q3, we find evidence that the top-left cohort, with markers of slower disease progression, has higher CE removal from the brain as indicated by higher levels of XL_HDL particle cholesterol and CE levels (**figure 5C**). We are confident that this peripheral measure of XL_HDL cholesterol has its origin in the CNS as this particle size has very low prevalence in the periphery but is the same particle size (13-18 nm diameter) as observed in CSF measurements of lipoprotein particle size (~14-17 nm diameter) (**figure 9**)[36]. Calculations from Nelson *et al* imply a 70% increase in CE/particle between mean APOE34 AD patients and controls in CNS lipoprotein particles[36].

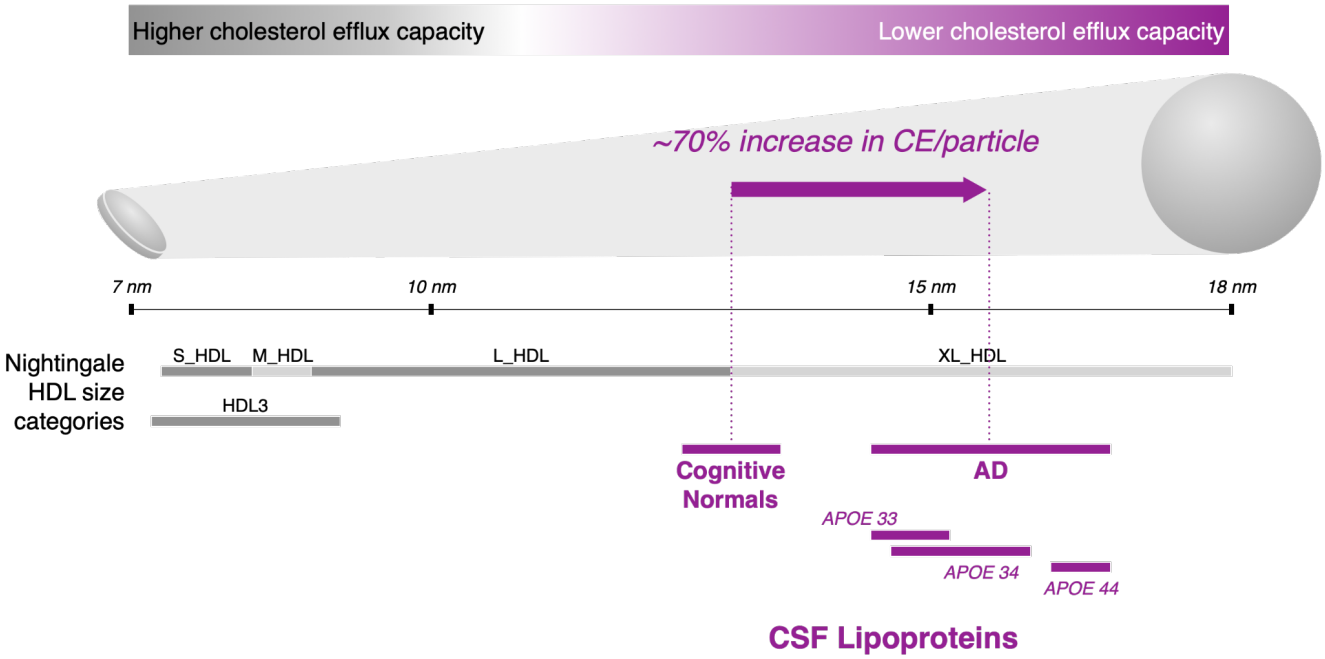

Figure 10: *Schematic depiction of CSF lipoprotein particles and relative efflux capacity and the differences in particle size distribution between cognitively normal and AD individuals.*

Our data in Q2 show that cellular responses to elevated cholesterol precede astrogliosis, with overload of the one-particle class HDL lipoprotein system driving AD pathology in early stages, prior to reaching the upper limits of microglial flux capacity in Q3. Using our lens of the one-particle class system and how it creates a fundamental conflict between debris management and cholesterol homeostasis, we can better understand how many known risk factors contribute to AD etiology. A study looking at the impact of sleep on RCT found that sleep loss decreased the expression of genes encoding cholesterol transporters and increased expression in pathways involved in inflammatory responses, resulting in lower circulating large HDL[83]. In a large study looking at PC intake, individuals with the highest PC intake levels had a 28% lower risk of dementia[84]. Greater numbers of small HDL particles (high carrying capacity) were positively associated with cognition[85]. Deficiency in vitamin D, a modulator of INSIG2/SREBP2 pathway, is associated with an increased risk of dementia[86,87]. Higher plasma omega-3s (DHA) reduces dementia risk[88]. [PLACEHOLDER FOR ADDITIONAL COMMENTARY ON GWAS RISK]

Our overall approach was to organize the multiomic data into a framework that enabled us to observe many of the underlying molecular processes of disease progression in Alzheimer's. There are many aspects of disease etiology and progression we do not address here. These include the factors that kick off the destabilizing feedback and likely begin pathology. While we do not address this, we feel they likely center around cerebral perfusion. As the brain is not evenly perfused, vulnerable regions are areas with poorer profusion, and include the hippocampus and subregions of the temporal cortex[89,90]. With loss of neurons in vulnerable regions, this increases synaptic compensation by the remaining neurons, increasing metabolic demand[91]. These are among the areas of interest we intend to explore in future studies.

Acknowledgements

Data collection and sharing for the Alzheimer's Disease Neuroimaging Initiative (ADNI) is funded by the National Institute on Aging (National Institutes of Health Grant U19 AG024904). The grantee organization is the Northern California Institute for Research and Education. In the past, ADNI has also

received funding from the National Institute of Biomedical Imaging and Bioengineering, the Canadian Institutes of Health Research, and private sector contributions through the Foundation for the National Institutes of Health (FNIH) including generous contributions from the following: AbbVie, Alzheimer's Association; Alzheimer's Drug Discovery Foundation; Araclon Biotech; BioClinica, Inc.; Biogen; Bristol-Myers Squibb Company; CereSpir, Inc.; Cogstate; Eisai Inc.; Elan Pharmaceuticals, Inc.; Eli Lilly and Company; EuroImmun; F. Hoffmann-La Roche Ltd and its affiliated company Genentech, Inc.; Fujirebio; GE Healthcare; IXICO Ltd.; Janssen Alzheimer Immunotherapy Research & Development, LLC.; Johnson & Johnson Pharmaceutical Research &Development LLC.; Lumosity; Lundbeck; Merck & Co., Inc.; Meso Scale Diagnostics, LLC.; NeuroRx Research; Neurotrack Technologies; Novartis Pharmaceuticals Corporation; Pfizer Inc.; Piramal Imaging; Servier; Takeda Pharmaceutical Company; and Transition Therapeutics.

Metabolomics Consortium (ADMC)

Data collection and sharing for this project was funded by the Alzheimer's Disease Metabolomics Consortium (National Institute on Aging R01AG046171, RF1AG051550 and 3U01AG024904-09S4).

Bibliography

1. Foley, P. (2010). Lipids in Alzheimer's disease: A century-old story. Biochim. Biophys. Acta (BBA) - Mol. Cell Biol. Lipids *1801*, 750–753. https://doi.org/10.1016/j.bbalip.2010.05.004.
2. Sims, J.R., Zimmer, J.A., Evans, C.D., Lu, M., Ardayfio, P., Sparks, J., Wessels, A.M., Shcherbinin, S., Wang, H., Nery, E.S.M., et al. (2023). Donanemab in Early Symptomatic Alzheimer Disease. JAMA *330*, *512*–527. https://doi.org/10.1001/jama.2023.*13239*.
3. Zhao, N., Ren, Y., Yamazaki, Y., Qiao, W., Li, F., Felton, L.M., Mahmoudiandehkordi, S., Kueider-Paisley, A., Sonoustoun, B., Arnold, M., et al. (2020). Alzheimer's Risk Factors Age, APOE Genotype, and Sex Drive Distinct Molecular Pathways. Neuron *106*, 727-742.e6. https://doi.org/10.1016/j.neuron.2020.02.034.
4. Romero-Molina, C., Garretti, F., Andrews, S.J., Marcora, E., and Goate, A.M. (2022). Microglial efferocytosis: Diving into the Alzheimer's disease gene pool. Neuron *110*, 3513–3533. https://doi.org/10.1016/j.neuron.2022.10.0*15*.
5. Alzheimer, A., Stelzmann, R.A., Schnitzlein, H.N., and Murtagh, F.R. (*1995*). An english translation of alzheimer's 1907 paper, "über eine eigenartige erkankung der hirnrinde." Clin. Anat. 8, 4*29*–*43*1. https://doi.org/10.1002/ca.980080612.
6. Ralhan, I., Chang, C.-L., Lippincott-Schwartz, J., and Ioannou, M.S. (2021). Lipid droplets in the nervous system. J. Cell Biol. *220*, e202102136. https://doi.org/10.1083/jcb.202102136.
7. Abildayeva, K., Jansen, P.J., Hirsch-Reinshagen, V., Bloks, V.W., Bakker, A.H.F., Ramaekers, F.C.S., Vente, J. de, Groen, A.K., Wellington, C.L., Kuipers, F., et al. (2006). 24(S)-Hydroxycholesterol Participates in a Liver X Receptor-controlled Pathway in Astrocytes That Regulates Apolipoprotein E-mediated Cholesterol Efflux. J Biol Chem *281*, 12799–12808. https://doi.org/10.1074/jbc.m*60*1019200.
8. Matsuda, A., Nagao, K., Matsuo, M., Kioka, N., and Ueda, K. (*2013*). 24(S)-hydroxycholesterol is actively eliminated from neuronal cells by ABCA1. J Neurochem *126*, *93*–101. https://doi.org/10.1111/jnc.1*2275*.
9. Fu, X., Menke, J.G., Chen, Y., Zhou, G., MacNaul, K.L., Wright, S.D., Sparrow, C.P., and Lund, E.G. (2001). 27-Hydroxycholesterol Is an Endogenous Ligand for Liver X Receptor in Cholesterol-loaded Cells*. J. Biol. Chem. *276*, 38*378*–38387. https://doi.org/10.1074/jbc.m*105*805200.
10. TCW, J., Qian, L., Pipalia, N.H., Chao, M.J., Liang, S.A., Shi, Y., Jain, B.R., Bertelsen, S.E., Kapoor, M., Marcora, E., et al. (2022). Cholesterol and matrisome pathways dysregulated in

astrocytes and microglia. Cell *185*, 2213-2233.e25. https://doi.org/10.1016/j.cell.2022.05.0*17*.
11. Smolič, T., Zorec, R., and Vardjan, N. (2021). Pathophysiology of Lipid Droplets in Neuroglia. Antioxidants 11, 22. https://doi.org/10.3390/antiox11010022.
12. Gamba, P., Staurenghi, E., Testa, G., Giannelli, S., Sottero, B., and Leonarduzzi, G. (2019). A Crosstalk Between Brain Cholesterol Oxidation and Glucose Metabolism in Alzheimer's Disease. Front Neurosci-switz 13, 556. https://doi.org/10.33*89*/fnins.2019.00556.
13. Leoni, V., and Caccia, C. (2011). Oxysterols as biomarkers in neurodegenerative diseases. Chem Phys Lipids *164*, 515–524. https://doi.org/10.1016/j.chemphyslip.2011.04.002.
***14*. Prasanna, X., Sengupta, D., and Chattopadhyay, A. (*2016*). Cholesterol-dependent Conformational Plasticity in GPCR Dimers. Sci Rep-uk 6, 31858. https://doi.org/10.1038/srep31858.**
15. Guixà-González, R., Albasanz, J.L., Rodriguez-Espigares, I., Pastor, M., Sanz, F., Martí-Solano, M., Manna, M., Martinez-Seara, H., Hildebrand, P.W., Martín, M., et al. (2017). Membrane cholesterol access into a G-protein-coupled receptor. Nat Commun 8, 14505. https://doi.org/10.1038/ncomms14505.
16. McGraw, C., Yang, L., Levental, I., Lyman, E., and Skaja-Robinson, A. (2019). Membrane cholesterol depletion reduces downstream signaling activity of the adenosine A2a receptor. Biochimica Et Biophysica Acta Bba - Biomembr *1861*, 760–767. https://doi.org/10.1016/j.bbamem.2019.01.001.
17. Prasanna, X., Mohole, M., Chattopadhyay, A., and Sengupta, D. (2020). Role of cholesterol-mediated effects in GPCR heterodimers. Chem Phys Lipids 227, 104852. https://doi.org/10.1016/j.chemphyslip.2019.104852.
18. Horvat, A., Zorec, R., and Vardjan, N. (2021). Lactate as an Astroglial Signal Augmenting Aerobic Glycolysis and Lipid Metabolism. Front. Physiol. 12, 735532. https://doi.org/10.3389/fphys.2021.735532.
19. Morland, C., Lauritzen, K.H., Puchades, M., Holm-Hansen, S., Andersson, K., Gjedde, A., Attramadal, H., Storm-Mathisen, J., and Bergersen, L.H. (2015). The lactate receptor, G-protein-coupled receptor 81/hydroxycarboxylic acid receptor 1: Expression and action in brain. J. Neurosci. Res. 93, 1045–1055. https://doi.org/10.1002/jnr.23593.
20. Hertz, L., Gibbs, M.E., and Dienel, G.A. (2014). Fluxes of lactate into, from, and among gap junction-coupled astrocytes and their interaction with noradrenaline. Front Neurosci-switz 8, 261. https://doi.org/10.3389/fnins.2014.00261.
21. Lange, Y., and Steck, T.L. (2016). Active membrane cholesterol as a physiological effector. Chem Phys Lipids 199, 74–93. https://doi.org/10.1016/j.chemphyslip.2016.02.003.
22. Javanainen, M., Enkavi, G., Guixà-Gonzaléz, R., Kulig, W., Martinez-Seara, H., Levental, I., and Vattulainen, I. (2019). Reduced level of docosahexaenoic acid shifts GPCR neuroreceptors to less ordered membrane regions. Plos Comput Biol 15, e1007033. https://doi.org/10.137*1*/journal.pcbi.1007033.
23. Haney, M.S., Pálovics, R., Munson, C.N., Long, C., Johansson, P.K., Yip, O., Dong, W., Rawat, E., West, E., Schlachetzki, J.C.M., et al. (2024). APOE4/4 is linked to damaging lipid droplets in Alzheimer's disease microglia. Nature, 1–8. https://doi.org/10.1038/s41586-024-07185-7.
24. Victor, M.B., Leary, N., Luna, X., Meharena, H.S., Scannail, A.N., Bozzelli, P.L., Samaan, G., Murdock, M.H., Maydell, D. von, Effenberger, A.H., et al. (2022). Lipid accumulation induced by APOE4 impairs microglial surveillance of neuronal-network activity. Cell Stem Cell 29, 11*97-121*2.e8. https://doi.org/10.1016/j.stem.2022.07.005.
25. TCW, J., Qian, L., Pipalia, N.H., Chao, M.J., Liang, S.A., Shi, Y., Jain, B.R., Bertelsen, S.E., Kapoor, M., Marcora, E., et al. (2022). Cholesterol and matrisome pathways dysregulated in astrocytes and microglia. Cell 185, 2213-2233.e25. https://doi.org/10.1016/j.cell.2022.05.017.
26. Nugent, A.A., Lin, K., Lengerich, B. van, Lianoglou, S., Przybyla, L., Davis, S.S., Llapashtica,

C., Wang, J., Kim, D.J., Xia, D., et al. (2020). TREM2 Regulates Microglial Cholesterol Metabolism upon Chronic Phagocytic Challenge. Neuron 105, 837-854.e9. https://doi.org/10.1016/j.neuron.2019.12.007.
27. Huynh, K., Lim, W.L.F., Giles, C., Jayawardana, K.S., Salim, A., Mellett, N.A., Smith, A.A.T., Olshansky, G., Drew, B.G., Chatterjee, P., et al. (2020). Concordant peripheral lipidome signatures in two large clinical studies of Alzheimer's disease. Nat Commun 11, 5698. https://doi.org/10.1038/s41467-020-19473-7.
28. Haque, R., Watson, C.M., Liu, J., Carter, E.K., Duong, D.M., Lah, J.J., Wingo, A.P., Roberts, B.R., Johnson, E.C.B., Saykin, A.J., et al. (2023). A protein panel in cerebrospinal fluid for diagnostic and predictive assessment of Alzheimer's disease. Sci. Transl. Med. 15, eadg4122. https://doi.org/10.1126/scitranslmed.adg4122.
29. Cruchaga, C., Ali, M., Shen, Y., Do, A., Wang, L., Western, D., Liu, M., Beric, A., Budde, J., Gentsch, J., et al. (2024). Multi-cohort cerebrospinal fluid proteomics identifies robust molecular signatures for asymptomatic and symptomatic Alzheimer's disease. Res. Sq., rs.3.rs-3631708. https://doi.org/10.21203/rs.3.rs-3631708/v1.
30. Landstra, E.N., Lohner, V., and Breteler, M.M.B. (2023). Sex-specific effects of Ceramides on White Matter Hyperintensities in the Rhineland Study. Alzheimer's Dement. 19. https://doi.org/10.1002/alz.078169.
31. Mielke, M.M., Syrjanen, J.A., Bui, H.H., Petersen, R.C., Knopman, D.S., Jr, C.R.J., Graff-Radford, J., and Vemuri, P. (2019). Elevated Plasma Ceramides Are Associated With Higher White Matter Hyperintensity Volume—Brief Report. Arter., Thromb., Vasc. Biol. 39, 2431–2436. https://doi.org/10.1161/atvbaha.119.313099.
32. Geng, B., Pan, J., Zhao, T., Ji, J., Zhang, C., Che, Y., Yang, J., Shi, H., Li, J., Zhou, H., et al. (2018). Chitinase 3-like 1-CD44 interaction promotes metastasis and epithelial-to-mesenchymal transition through β-catenin/Erk/Akt signaling in gastric cancer. J. Exp. Clin. Cancer Res. 37, 208. https://doi.org/10.1186/s13046-018-0876-2.
33. Connolly, K., Lehoux, M., O'Rourke, R., Assetta, B., Erdemir, G.A., Elias, J.A., Lee, C.G., and Huang, Y.A. (2023). Potential role of chitinase-3-like protein 1 (CHI3L1/YKL-40) in neurodegeneration and Alzheimer's disease. Alzheimer's Dement. 19, 9–24. https://doi.org/10.1002/alz.12612.
34. Satoh, J., Yamamura, T., and Arima, K. (2004). The 14-3-3 Protein ε Isoform Expressed in Reactive Astrocytes in Demyelinating Lesions of Multiple Sclerosis Binds to Vimentin and Glial Fibrillary Acidic Protein in Cultured Human Astrocytes. Am. J. Pathol. *165*, 577–592. https://doi.org/10.1016/s0002-9440(10)63322-6.
35. Shimada, T., Fournier, A.E., and Yamagata, K. (2013). Neuroprotective Function of 14-3-3 Proteins in Neurodegeneration. BioMed Res. Int. 2013, 564534. https://doi.org/10.1155/2013/564534.
36. Nelson, T.J., and Sen, A. (2018). Apolipoprotein E particle size is increased in Alzheimer's disease. Alzheimer's Dementia Diagnosis Assess Dis Monit 11, 10–18. https://doi.org/10.1016/j.dadm.2018.10.005.
37. Arendt, T., Brückner, M.K., Morawski, M., Jäger, C., and Gertz, H.-J. (2015). Early neurone loss in Alzheimer's disease: cortical or subcortical? Acta Neuropathol. Commun. 3, 10. https://doi.org/10.1186/s40478-015-0187-1.
38. Kerdiles, O., Layé, S., and Calon, F. (2017). Omega-3 polyunsaturated fatty acids and brain health: Preclinical evidence for the prevention of neurodegenerative diseases. Trends Food Sci. Technol. 69, 203–213. https://doi.org/10.1016/j.tifs.2017.09.003.
39. Burckhardt, M., Herke, M., Wustmann, T., Watzke, S., Langer, G., and Fink, A. (2016). Omega-3 fatty acids for the treatment of dementia. Cochrane Database Syst. Rev. 2016, CD009002. https://doi.org/10.1002/14651858.cd009002.pub3.

40. Desale, S.E., and Chinnathambi, S. (2020). Role of dietary fatty acids in microglial polarization in Alzheimer's disease. J. Neuroinflammation 17, 93. https://doi.org/10.1186/s12974-020-01742-3.
41. Schacky, C. von (2020). Omega-3 index in 2018/19. Proc. Nutr. Soc. 79, 381–387. https://doi.org/10.1017/s0029665120006989.
42. Schuchardt, J.P., Tintle, N., Westra, J., and Harris, W.S. (2023). Estimation and predictors of the Omega-3 Index in the UK Biobank. Br. J. Nutr. 130, 312–322. https://doi.org/10.1017/s0007114522003282.
43. Schacky, C. von (2014). Omega-3 Index and Cardiovascular Health. Nutrients 6, 799–814. https://doi.org/10.3390/nu6020799.
44. Tang, H., Liu, Z., Han, G., Geng, J., Liu, B., Zhang, R., and Zhang, Z. (2024). Unexpected omega-3 activities in intracellular lipolysis and macrophage foaming revealed by fluorescence lifetime imaging. Proc. Natl. Acad. Sci. 121, e2321255121. https://doi.org/10.1073/pnas.2321255121.
45. Barber, E., Sinclair, A.J., and Cameron-Smith, D. (2013). Comparative actions of omega-3 fatty acids on in-vitro lipid droplet formation. Prostaglandins, Leukot. Essent. Fat. Acids (PLEFA) 89, 359–366. https://doi.org/10.1016/j.plefa.2013.07.006.
46. Ferdinandusse, S., and Houten, S.M. (2006). Peroxisomes and bile acid biosynthesis. Biochim. Biophys. Acta (BBA) - Mol. Cell Res. *1763*, *1427*–1440. https://doi.org/10.1016/j.bbamcr.2006.09.001.
47. Schott, J.M., Crutch, S.J., Carrasquillo, M.M., Uphill, J., Shakespeare, T.J., Ryan, N.S., Yong, K.X., Lehmann, M., Ertekin-Taner, N., Graff-Radford, N.R., et al. (2016). Genetic risk factors for the posterior cortical atrophy variant of Alzheimer's disease. Alzheimer's Dementia 12, 862–871. https://doi.org/10.1016/j.jalz.2016.01.010.
48. Yeoh, W.J., and Krebs, P. (2023). SHIP1 and its role for innate immune regulation—Novel targets for immunotherapy. Eur. J. Immunol. 53, e2350446. https://doi.org/10.1002/eji.202350446.
49. Suthar, S.K., Alam, M.M., Lee, J., Monga, J., Joseph, A., and Lee, S.-Y. (2021). Bioinformatic Analyses of Canonical Pathways of TSPOAP1 and its Roles in Human Diseases. Front. Mol. Biosci. 8, 667947. https://doi.org/10.3389/fmolb.2021.667947.
50. Tchoua, U., Gillard, B.K., and Pownall, H.J. (2010). HDL superphospholipidation enhances key steps in reverse cholesterol transport. Atherosclerosis *209*, 430–435. https://doi.org/10.1016/j.atherosclerosis.2009.10.002.
51. Cole, L.K., Vance, J.E., and Vance, D.E. (2012). Phosphatidylcholine biosynthesis and lipoprotein metabolism. Biochimica Et Biophysica Acta Bba - Mol Cell Biology Lipids *1821*, 754–761. https://doi.org/10.1016/j.bbalip.2011.09.009.
52. Chamberlain, K.A., and Sheng, Z. (2019). Mechanisms for the maintenance and regulation of axonal energy supply. J. Neurosci. Res. 97, 897–913. https://doi.org/10.1002/jnr.24411.
53. Coggan, J.S., Keller, D., Calì, C., Lehväslaiho, H., Markram, H., Schürmann, F., and Magistretti, P.J. (2018). Norepinephrine stimulates glycogenolysis in astrocytes to fuel neurons with lactate. Plos Comput Biol 14, e1006392. https://doi.org/10.1371/journal.pcbi.1006392.
54. Dimsdale, J.E., O'Connor, D.T., Ziegler, M., and Mills, P. (1992). Chromogranin a correlates with norepinephrine release rate. Life Sci. 51, 519–525. https://doi.org/10.1016/0024-3205(92)90029-o.
55. Dumitrescu, L., Mahoney, E.R., Mukherjee, S., Lee, M.L., Bush, W.S., Engelman, C.D., Lu, Q., Fardo, D.W., Trittschuh, E.H., Mez, J., et al. (2020). Genetic variants and functional pathways associated with resilience to Alzheimer's disease. Brain *143*, 2561–2575. https://doi.org/10.1093/brain/awaa209.
56. Young, V.G., Halliday, G.M., and Kril, J.J. (2008). Neuropathologic correlates of white matter hyperintensities. Neurology 71, 804–811. https://doi.org/10.1212/01.wnl.0000319691.50117.54.

57. Li, Y., Li, M., Zhang, X., Shi, Q., Yang, S., Fan, H., Qin, W., Yang, L., Yuan, J., Jiang, T., et al. (2017). Higher blood–brain barrier permeability is associated with higher white matter hyperintensities burden. J. Neurol. *264*, 1474–1481. https://doi.org/10.1007/s00415-017-8550-8.
58. COMPSTON, D.A.S., MORGAN, B.P., CAMPBELL, A.K., WILKINS, P., COLE, G., THOMAS, N.D., and JASANI, B. (1989). IMMUNOCYTOCHEMICAL LOCALIZATION OF THE TERMINAL COMPLEMENT COMPLEX IN MULTIPLE SCLEROSIS. Neuropathol. Appl. Neurobiol. 15, 307–316. https://doi.org/10.1111/j.1365-2990.1989.tb01231.x.
59. Elahi, F.M., Harvey, D., Altendahl, M., Brathaban, N., Fernandes, N., Casaletto, K.B., Staffaroni, A.M., Maillard, P., Hinman, J.D., Miller, B.L., et al. (2021). Elevated complement mediator levels in endothelial-derived plasma exosomes implicate endothelial innate inflammation in diminished brain function of aging humans. Sci. Rep. 11, 16198. https://doi.org/10.1038/s41598-021-91759-2.
60. Heinecke, J.W. (2009). The HDL proteome: a marker–and perhaps mediator–of coronary artery disease. J. Lipid Res. 50, S167–S171. https://doi.org/10.1194/jlr.r800097-jlr200.
61. Davidson, W.S., Shah, A.S., Sexmith, H., and Gordon, S.M. (2022). The HDL Proteome Watch: Compilation of studies leads to new insights on HDL function. Biochim. Biophys. Acta (BBA) - Mol. Cell Biol. Lipids *1867*, 159072. https://doi.org/10.1016/j.bbalip.2021.159072.
62. Parra, S., Vives, G., Ferré, R., González, M., Guardiola, M., Ribalta, J., and Castro, A. (2012). Complement system and small HDL particles are associated with subclinical atherosclerosis in SLE patients. Atherosclerosis *225*, 224–230. https://doi.org/10.1016/j.atherosclerosis.2012.08.029.
63. Hillmer, L., Erhardt, E.B., Caprihan, A., Adair, J.C., Knoefel, J.E., Prestopnik, J., Thompson, J., Hobson, S., and Rosenberg, G.A. (2022). Blood-brain barrier disruption measured by albumin index correlates with inflammatory fluid biomarkers. J. Cereb. Blood Flow Metab. 43, 712–721. https://doi.org/10.1*177*/0271678x221146127.
64. WADA, H. (2006). Blood-Brain Barrier Permeability of the Demented Elderly as Studied by Cerebrospinal Fluid-Serum Albumin Ratio. Intern. Med. 37, 509. https://doi.org/10.2169/internalmedicine.37.509.
65. Obinata, H., Kuo, A., Wada, Y., Swendeman, S., Liu, C.H., Blaho, V.A., Nagumo, R., Satoh, K., Izumi, T., and Hla, T. (2019). Identification of ApoA4 as a sphingosine 1-phosphate chaperone in ApoM- and albumin-deficient mice. J. Lipid Res. 60, 1912–1921. https://doi.org/10.1194/jlr.ra119000277.
66. Bartus, R.T., Elliott, P.J., Dean, R.L., Hayward, N.J., Nagle, T.L., Huff, M.R., Snodgrass, P.A., and Blunt, D.G. (1996). Controlled Modulation of BBB Permeability Using the Bradykinin Agonist, RMP-7. Exp. Neurol. 142, 14–28. https://doi.org/10.1006/exnr.1996.0175.
67. Castellazzi, M., Trentini, A., Romani, A., Valacchi, G., Bellini, T., Bonaccorsi, G., Fainardi, E., Cavicchio, C., Passaro, A., Zuliani, G., et al. (2016). Decreased arylesterase activity of paraoxonase-1 (PON-1) might be a common denominator of neuroinflammatory and neurodegenerative diseases. Int. J. Biochem. Cell Biol. 81, 356–363. https://doi.org/10.1016/j.biocel.2016.06.008.
68. Seres, I., Paragh, G., Deschene, E., Fulop, T., and Khalil, A. (2004). Study of factors influencing the decreased HDL associated PON1 activity with aging. Exp. Gerontol. 39, 59–66. https://doi.org/10.1016/j.exger.2003.08.001.
69. Chen, X., Firulyova, M., Manis, M., Herz, J., Smirnov, I., Aladyeva, E., Wang, C., Bao, X., Finn, M.B., Hu, H., et al. (2023). Microglia-mediated T cell infiltration drives neurodegeneration in tauopathy. Nature, 1–10. https://doi.org/10.1038/s41586-023-05788-0.
70. Nugent, A.A., Lin, K., Lengerich, B. van, Lianoglou, S., Przybyla, L., Davis, S.S., Llapashtica, C., Wang, J., Kim, D.J., Xia, D., et al. (2020). TREM2 Regulates Microglial Cholesterol Metabolism upon Chronic Phagocytic Challenge. Neuron 105, 837-854.e9. https://doi.org/10.1016/

j.neuron.2019.12.007.
71. Cignarella, F., Filipello, F., Bollman, B., Cantoni, C., Locca, A., Mikesell, R., Manis, M., Ibrahim, A., Deng, L., Benitez, B.A., et al. (2020). TREM2 activation on microglia promotes myelin debris clearance and remyelination in a model of multiple sclerosis. Acta Neuropathol *140*, 513–534. https://doi.org/10.1007/s00401-020-02193-z.
72. Pellerin, L., and Magistretti, P.J. (2011). Sweet Sixteen for ANLS. J. Cereb. Blood Flow Metab. 32, 1152–1166. https://doi.org/10.1038/jcbfm.2011.149.
73. Konishi, H., Okamoto, T., Hara, Y., Komine, O., Tamada, H., Maeda, M., Osako, F., Kobayashi, M., Nishiyama, A., Kataoka, Y., et al. (2020). Astrocytic phagocytosis is a compensatory mechanism for microglial dysfunction. Embo J 39, e104464. https://doi.org/10.15252/embj.2020104464.
74. Chaves, E.P. de, Narayanaswami, V., Christoffersen, C., and Nielsen, L.B. (2008). Apolipoprotein E and cholesterol in aging and disease in the brain. Futur. Lipidol. 3, 505–530. https://doi.org/10.2217/17460875.3.5.505.
75. Ioannou, M.S., Jackson, J., Sheu, S.-H., Chang, C.-L., Weigel, A.V., Liu, H., Pasolli, H.A., Xu, C.S., Pang, S., Matthies, D., et al. (2019). Neuron-Astrocyte Metabolic Coupling Protects against Activity-Induced Fatty Acid Toxicity. Cell 177, 1522-1535.e14. https://doi.org/10.1016/j.cell.2019.04.001.
76. Marquer, C., Laine, J., Dauphinot, L., Hanbouch, L., Lemercier-Neuillet, C., Pierrot, N., Bossers, K., Le, M., Corlier, F., Benstaali, C., et al. (2014). Increasing membrane cholesterol of neurons in culture recapitulates Alzheimer's disease early phenotypes. Mol. Neurodegener. 9, 60. https://doi.org/10.1186/1750-1326-9-60.
77. Grösgen, S., Grimm, M.O.W., Frieß, P., and Hartmann, T. (2010). Role of amyloid beta in lipid homeostasis. Biochimica Et Biophysica Acta Bba - Mol Cell Biology Lipids 1801, 966–974. https://doi.org/10.1016/j.bbalip.2010.05.002.
78. Wang, H., Kulas, J.A., Wang, C., Holtzman, D.M., Ferris, H.A., and Hansen, S.B. (2021). Regulation of beta-amyloid production in neurons by astrocyte-derived cholesterol. Proc. Natl. Acad. Sci. 118, e2102191118. https://doi.org/10.1073/pnas.2102191118.
79. Hong, B.V., Zheng, J., Agus, J.K., Tang, X., Lebrilla, C.B., Jin, L.-W., Maezawa, I., Erickson, K., Harvey, D.J., DeCarli, C.S., et al. (2022). High-Density Lipoprotein Changes in Alzheimer's Disease Are APOE Genotype-Specific. Biomed 10, 1495. https://doi.org/10.3390/biomedicines10071495.
80. Du, X.-M., Kim, M.-J., Hou, L., Goff, W.L., Chapman, M.J., Eck, M.V., Curtiss, L.K., Burnett, J.R., Cartland, S.P., Quinn, C.M., et al. (2015). HDL Particle Size Is a Critical Determinant of ABCA1-Mediated Macrophage Cellular Cholesterol Export. Circ Res 116, 1133–1142. https://doi.org/10.1161/circresaha.116.305485.
81. Yassine, H.N., Feng, Q., Chiang, J., Petrosspour, L.M., Fonteh, A.N., Chui, H.C., and Harrington, M.G. (2016). ABCA1-Mediated Cholesterol Efflux Capacity to Cerebrospinal Fluid Is Reduced in Patients With Mild Cognitive Impairment and Alzheimer's Disease. J. Am. Hear. Assoc. 5, e002886. https://doi.org/10.1161/jaha.115.002886.
82. Hong, B.V., Agus, J., Zheng, J.J., Lebrilla, C.B., Jin, L., Maezawa, I., Harvey, D.J., and Zivkovic, A.M. (2022). Altered HDL Cholesterol Efflux Capacity and LCAT Activity is APOE-Specific in Alzheimer Disease and Mild Cognitive Impairment Patients. Alzheimer's Dement. 18. https://doi.org/10.1002/alz.066086.
83. Aho, V., Ollila, H.M., Kronholm, E., Bondia-Pons, I., Soininen, P., Kangas, A.J., Hilvo, M., Seppälä, I., Kettunen, J., Oikonen, M., et al. (2016). Prolonged sleep restriction induces changes in pathways involved in cholesterol metabolism and inflammatory responses. Sci Rep-uk 6, 24828. https://doi.org/10.1038/srep24828.
84. Ylilauri, M.P.T., Voutilainen, S., Lönnroos, E., Virtanen, H.E.K., Tuomainen, T.-P., Salonen, J.T.,

and Virtanen, J.K. (2019). Associations of dietary choline intake with risk of incident dementia and with cognitive performance: the Kuopio Ischaemic Heart Disease Risk Factor Study. Am J Clin Nutrition 110, 1416–1423. https://doi.org/10.1093/ajcn/nqz148.
85. Martinez, A.E., Weissberger, G., Kuklenyik, Z., He, X., Meuret, C., Parekh, T., Rees, J.C., Parks, B.A., Gardner, M.S., King, S.M., et al. (2022). The small HDL particle hypothesis of Alzheimer's disease. Alzheimer's Dementia. https://doi.org/10.1002/alz.12649.
86. Navale, S.S., Mulugeta, A., Zhou, A., Llewellyn, D.J., and Hyppönen, E. (2022). Vitamin D and brain health: an observational and Mendelian randomization study. Am J Clin Nutrition 116, nqac107-. https://doi.org/10.1093/ajcn/nqac107.
87. Li, S., He, Y., Lin, S., Hao, L., Ye, Y., Lv, L., Sun, Z., Fan, H., Shi, Z., Li, J., et al. (2016). Increase of circulating cholesterol in vitamin D deficiency is linked to reduced vitamin D receptor activity via the Insig-2/SREBP-2 pathway. Mol Nutr Food Res 60, 798–809. https://doi.org/10.1002/mnfr.201500425.
88. Schaefer, E.J., Bongard, V., Beiser, A.S., Lamon-Fava, S., Robins, S.J., Au, R., Tucker, K.L., Kyle, D.J., Wilson, P.W.F., and Wolf, P.A. (2006). Plasma Phosphatidylcholine Docosahexaenoic Acid Content and Risk of Dementia and Alzheimer Disease: The Framingham Heart Study. Arch Neurol-chicago 63, 1545–1550. https://doi.org/10.1001/archneur.63.11.1545.
89. Shaw, K., Bell, L., Boyd, K., Grijseels, D.M., Clarke, D., Bonnar, O., Crombag, H.S., and Hall, C.N. (2021). Neurovascular coupling and oxygenation are decreased in hippocampus compared to neocortex because of microvascular differences. Nat Commun 12, 3190. https://doi.org/10.1038/s41467-021-23508-y.
90. Austin, B.P., Nair, V.A., Meier, T.B., Xu, G., Rowley, H.A., Carlsson, C.M., Johnson, S.C., and Prabhakaran, V. (2011). Effects of Hypoperfusion in Alzheimer's Disease. J. Alzheimer's Dis. 26, 123–133. https://doi.org/10.3233/jad-2011-0010.
91. Neuman, K.M., Molina-Campos, E., Musial, T.F., Price, A.L., Oh, K.-J., Wolke, M.L., Buss, E.W., Scheff, S.W., Mufson, E.J., and Nicholson, D.A. (2015). Evidence for Alzheimer's disease-linked synapse loss and compensation in mouse and human hippocampal CA1 pyramidal neurons. Brain Struct Funct 220, 3143–3165. https://doi.org/10.1007/s00429-014-0848-z.